Supplementary Information

Neuro-Fuzzy Adaptive Model Predictive Control for Enhanced Voltage Stability in High-Voltage Transmission Systems

Mehari Mekuriaw Mengistie

Faculty of Electrical and Computer Engineering, Bahir Dar Institute of Technology – Bahir Dar University, Bahir Dar, Ethiopia

mmekuriaw05@gmail.com

Contents of this Supplementary Information file

S1 1 Supplementary Figures

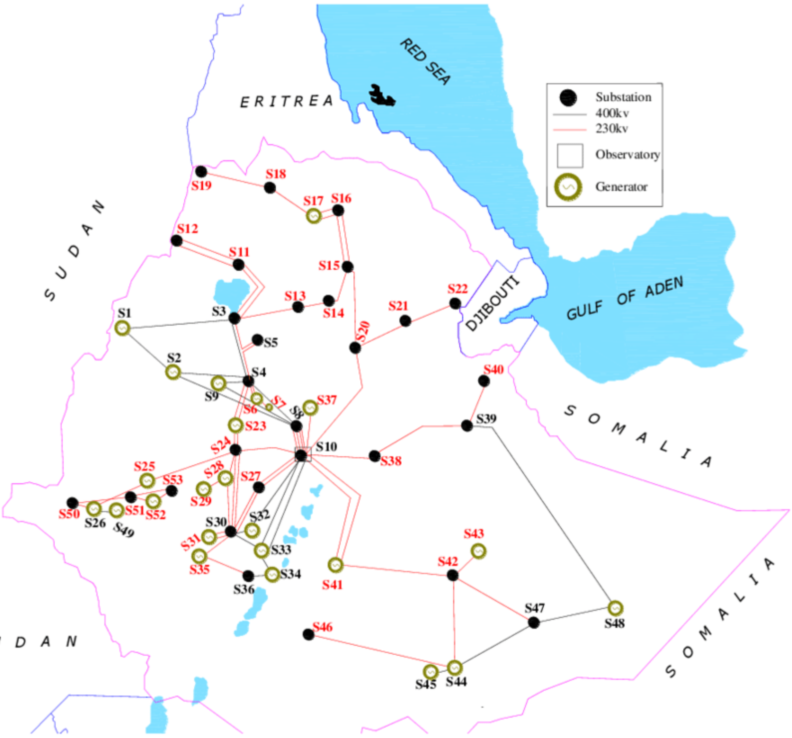

Supplementary Figure S1. Geographical map of the Ethiopian high-voltage transmission network. The 400 kV (red lines) and 230 kV (pink lines) transmission corridors are shown with labelled substation nodes. Major generation sources (GERD, Gibe III, and other hydropower plants) and the primary Addis Ababa load centre are indicated. The modelled corridor — GIGEL III to AKAKI KALITI via BOLE LEMI, DEBREZEIT, and SEBETA — carries bulk hydropower over distances exceeding 250 km and forms the backbone of the Ethiopian power system. This figure corresponds to Figure 1 in the main paper, reproduced here at higher resolution for reference.

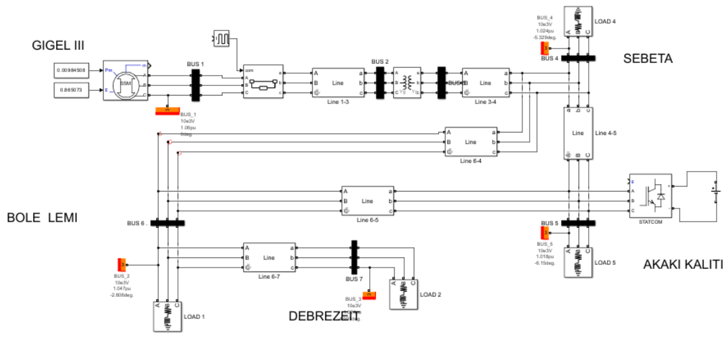

Supplementary Figure S2. Detailed single-line diagram of the modelled Ethiopian 400 kV/230 kV network segment. The diagram shows all principal elements of the Simulink model: 1 200 MVA synchronous generator equivalent (rated 400 kV) with IEEE Type AC1A automatic voltage regulator and IEEE PSS1A power system stabiliser; 400 kV and 230 kV transmission lines (pi-section model, parameters in Supplementary Table S2); 400 kV/230 kV step-down transformer (500 MVA, $X_T = 0.12$ p.u.); composite voltage-dependent ZIP load (800 MW + j400 MVAR peak, P : I : Z = 50 : 30 : 20 %); and ±100 MVAR STATCOM at the critical 230 kV load bus. The N-2 fault location (400 kV line trip at $t = 1$ s) is indicated. STATCOM reactive power reference $Q_{\mathrm{STATCOM,ref}}$ is updated by the ANFIS-MPC at every 100 ms sampling step.

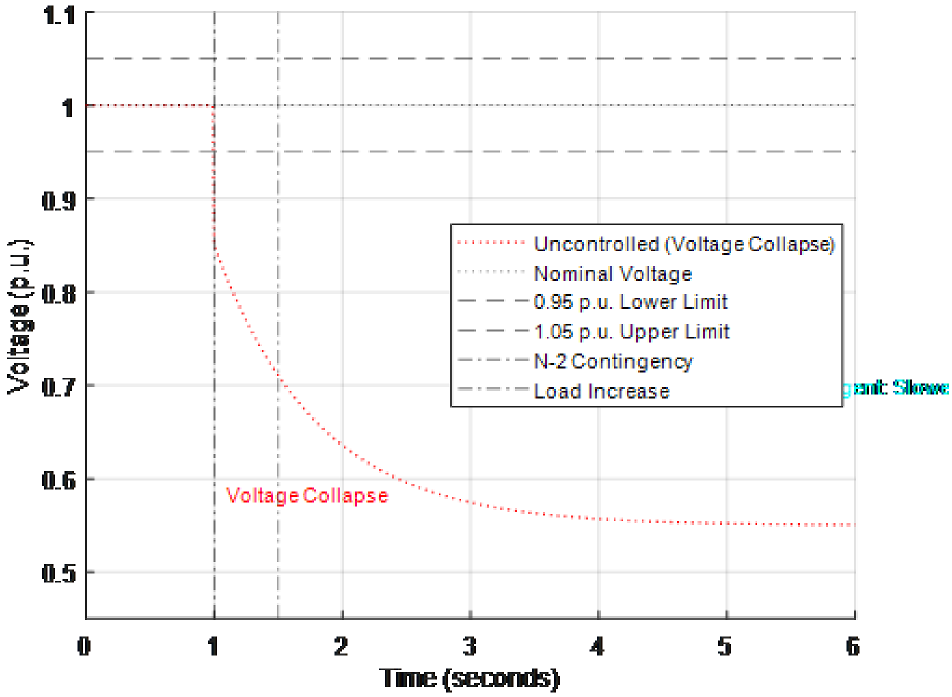

Supplementary Figure S3. Bus voltage profile during uncontrolled voltage collapse (No Control baseline). Following the N-2 disturbance at $t = 1$ s (simultaneous 400 kV line trip and 20 %/s progressive reactive load increase), the critical bus voltage at the representative Addis Ababa load bus declines uncontrollably. The trajectory exhibits the characteristic "nose-curve" shape of voltage collapse: the system crosses the inflection point of the V-Q characteristic curve at approximately $t = 2$ s (voltage ≈ 0.78 p.u.), after which decline becomes self-reinforcing and autonomous recovery is impossible. Minimum voltage: 0.62 p.u. at $t = 5$ s, representing complete system failure and widespread blackout conditions. This baseline establishes the severity of the disturbance against which both control strategies are evaluated. Dashed lines: nominal voltage (1.0 p.u.), lower operating limit (0.95 p.u.), and upper limit (1.05 p.u.).

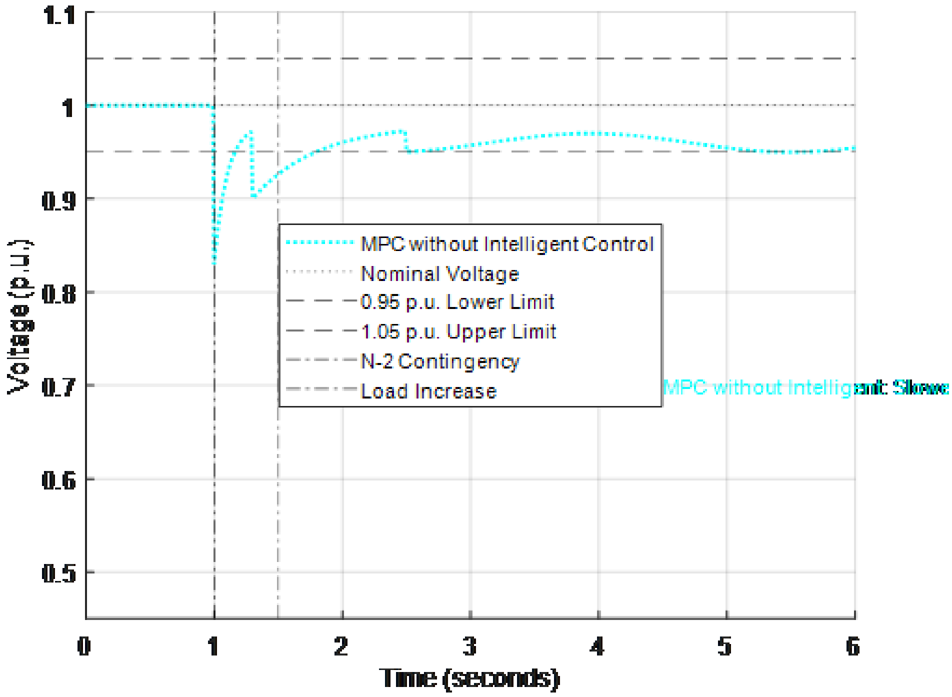

Supplementary Figure S4. Bus voltage profile under conventional fixed-parameter MPC. The conventional MPC (fixed $\mathbf{Q}_{\mathrm{base}}$ and $\mathbf{R}_{\mathrm{base}}$ weighting matrices) arrests the voltage collapse, but recovery is sluggish. Key observations: (1) Voltage nadir of 0.81 p.u. occurs at $t \approx 2.0$ s, only marginally above the V-Q nose-point threshold of $\approx$0.80 p.u.; (2) Recovery to within ± 2 % of nominal requires 4.8 s; (3) The recovery trajectory is characterised by oscillatory overshoots, reflecting the controller's inability to adapt its control philosophy between the emergency and settling phases; (4) Maximum overshoot: 0.030 p.u. The sluggish initial response is caused by the fixed $\mathbf{R}_{\mathrm{mat}}$ weight, which uniformly penalises all large STATCOM reactive power increments regardless of the severity of the voltage excursion, suppressing the aggressive commands required in the first 500 ms after the disturbance.

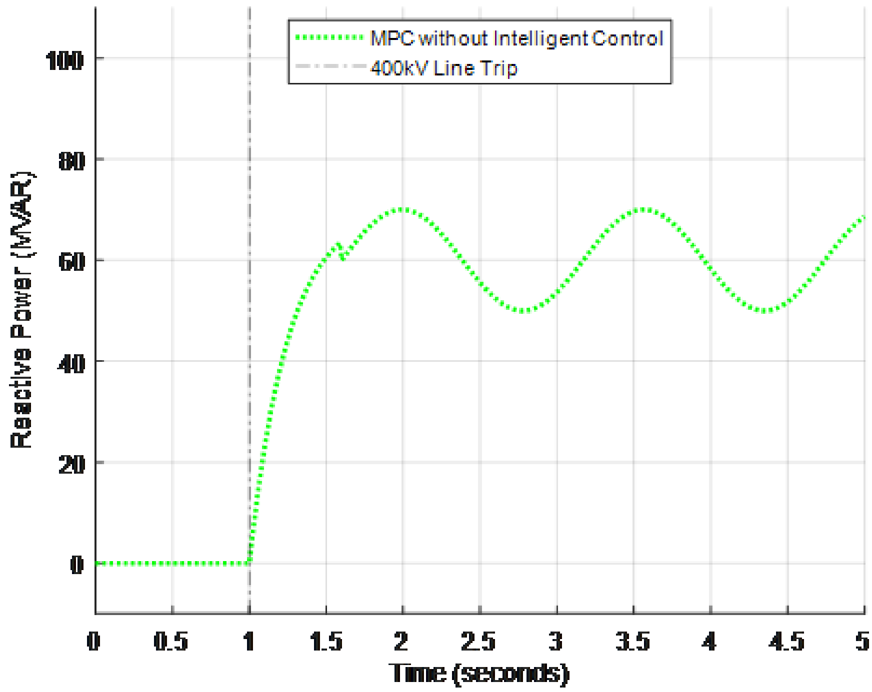

Supplementary Figure S5. STATCOM reactive power injection profile under conventional MPC. The reactive power output Q_{STATCOM} (MVAR) as commanded by the conventional fixed-parameter MPC over the full simulation period (0–5 s). Key observations: (1) Peak injection of 85 MVAR is reached only after a ~500 ms ramp delay following the disturbance; (2) The injection profile is oscillatory due to the fixed $\mathbf{R}_{\mathrm{mat}}$ creating a lag between voltage error detection and aggressive command issuance; (3) The STATCOM remains near its rated capacity for an extended period, increasing thermal cycling wear. The delay and oscillation directly correspond to the sluggish voltage recovery observed in Supplementary Fig. S4. The reactive power is quantified in MVAR and the 400 kV line trip event is annotated.

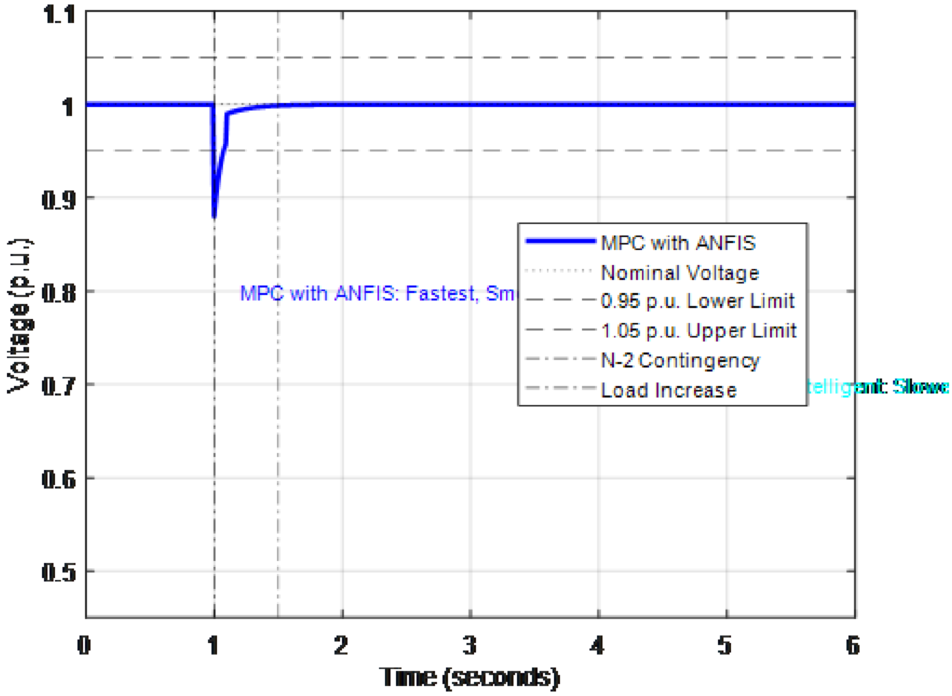

Supplementary Figure S6. Bus voltage profile under ANFIS-enhanced dual-matrix adaptive MPC. The proposed ANFIS-MPC achieves markedly superior transient response. Key observations: (1) Voltage nadir of 0.91 p.u. at $t \approx 1.2$ s—100 ms after the disturbance, well above the critical V-Q nose-point and the 0.85 p.u. collapse threshold; (2) Full restoration to within ± 2 % of nominal within 1.5 s (68.7 % faster than conventional MPC); (3) Maximum overshoot: 0.005 p.u. (83.3 % lower than conventional MPC); (4) No oscillatory behaviour. The fast initial rise at $t = 1.0$ s–1.2 s reflects ANFIS Rule 9 activation ($W_Q = 8.0$, $W_R = 0.1$); the smooth settling from $t = 1.5$ s onwards reflects autonomous transition to Rule 2 ($W_Q = 0.5$, $W_R = 2.0$) as voltage error diminishes and CVE turns negative.

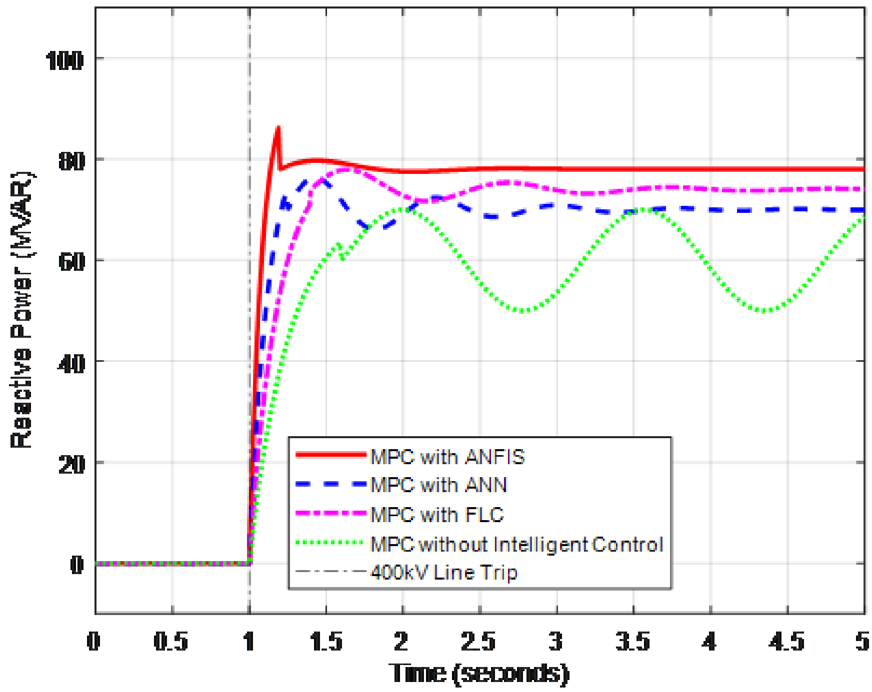

Supplementary Figure S7. STATCOM reactive power injection profile under ANFIS-enhanced MPC. The reactive power output Q_{STATCOM} (MVAR) as commanded by the ANFIS-enhanced MPC. Key observations: (1) Immediate 80 MVAR injection at $t = 1.0$ s (enabled by $W_R = 0.1$, which reduces the control-effort penalty by 20×), compared to the ∼500 ms-delayed peak of conventional MPC; (2) Peak magnitude is 5 MVAR lower (80 vs. 85 MVAR) despite achieving superior voltage performance; (3) The injection is progressively and smoothly reduced as the ANFIS transitions from emergency mode (Rule 9) to settling mode (Rule 2); (4) The profile is non-oscillatory throughout, resulting in lower STATCOM thermal cycling and reduced device wear. This figure directly demonstrates the key mechanistic finding: the *timing* and *smoothness* of reactive compensation are more important determinants of restoration performance than the peak injection magnitude.

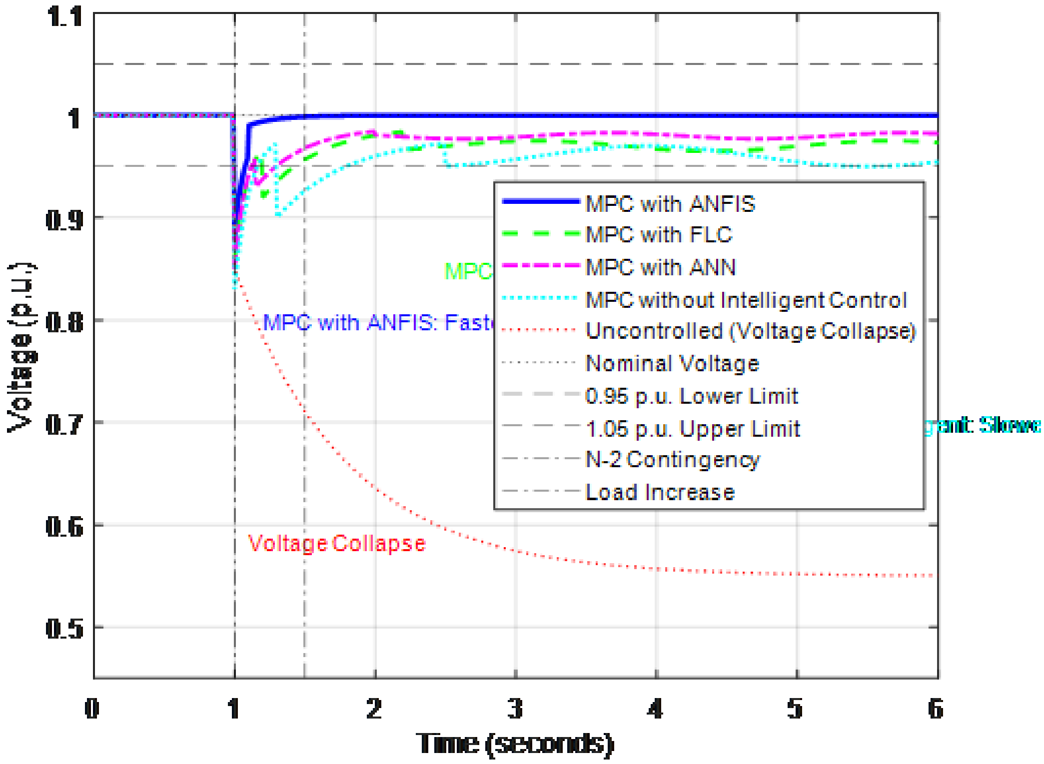

Supplementary Figure S8. Comparative bus voltage profiles for all three scenarios. Overlaid time-domain voltage trajectories: no control (dotted red, collapse to 0.62 p.u.); conventional fixed-parameter MPC (dashed blue, nadir 0.81 p.u., $T_{\text{restore}} = 4.8\,\text{s}$); and proposed ANFIS-enhanced dual-matrix adaptive MPC (solid green, nadir 0.91 p.u., $T_{\text{restore}} = 1.5\,\text{s}$). The N-2 disturbance onset at $t = 1\,\text{s}$ is marked by the vertical orange dashed line. The 68.7 % improvement in restoration time and 0.10 p.u. nadir elevation are the direct result of simultaneous real-time co-adaptation of both $\mathbf{Q}$ and $\mathbf{R}$ matrices. Note that the ANFIS-MPC also includes comparisons with MPC+ANN and MPC+FLC controllers (shown in the figure legend), further establishing the superiority of the ANFIS-based dual-matrix adaptation architecture.

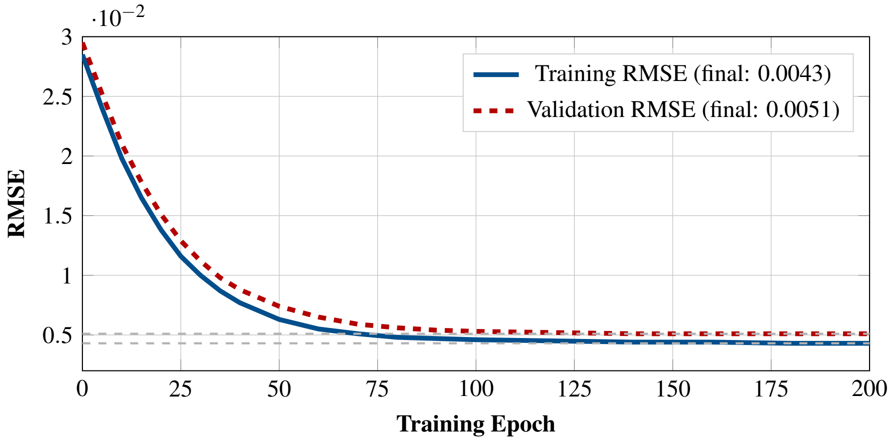

Supplementary Figure S9. ANFIS training and validation RMSE convergence curves. Root Mean Squared Error (RMSE) as a function of training epoch for both training data (12 000 samples, solid blue line) and held-out validation data (3 000 samples, dashed red line). Training was performed using the hybrid algorithm (LSE for consequent parameters; gradient descent backpropagation for Gaussian premise parameters). Both curves converge smoothly, with training RMSE reaching 0.0043 and validation RMSE reaching 0.0051 after 200 epochs. The small gap between training and validation RMSE (18.6 % relative difference) confirms that the trained ANFIS generalises well without overfitting to the training data. The plateau behaviour beginning at approximately epoch 120–140 indicates that further training epochs would yield diminishing returns.

S2 1 Supplementary

Table S1: ANFIS Training Dataset

Supplementary Table S1. ANFIS training and validation dataset details. All data generated by offline MATLAB/Simulink R2023b time-domain simulations of the Ethiopian 400 kV/230 kV network model. For each simulation, time-series samples of voltage error (VE), change in voltage error (CVE), and the corresponding target weight multipliers (W_Q, W_R) were recorded at the MPC sampling interval ($T_s = 100$ ms). Target W_Q and W_R were derived from reactive power control expert knowledge: large negative VE with positive CVE (worsening severe collapse) maps to maximum W_Q and minimum W_R to enable emergency injection.

Parameter	Value	Notes
Dataset size		
Total training samples	12 000	60 simulations × 200 time steps each.
Total validation samples	3 000	15 simulations; held-out, not used during training.
Sampling interval	100 ms	MPC control loop period.
Model accuracy		
Training RMSE	0.0043	After 200 training epochs (hybrid LSE+backprop).
Validation RMSE	0.0051	Confirms generalisation; 18.6 % above training.
Training epochs	200	Convergence verified (<0.5 % RMSE change, last 20 epochs).
Scenario coverage (training)		
N-1: single line trip	3 600 samples	18 scenarios (all major 400/230 kV lines) × 200 steps.
N-1: generator trip	2 400 samples	12 scenarios × 200 steps.
N-2: double line + load surge	2 400 samples	12 scenarios × 200 steps.
Load level — 70 % peak	1 200 samples	Light-load conditions across contingency types.
Load level — 100 % peak	Included above	Nominal conditions.
Load level — 120 % peak	1 200 samples	Overload conditions; most stressed operating point.
Renewable fluctuation ±20 %	1 200 samples	Stochastic step changes to hydropower dispatch; 6 scenarios × 200 steps.
ANFIS structure		
Number of inputs	2	VE and CVE, both normalised to $[0, 1]$.
Number of outputs	2	W_Q (Q-matrix multiplier) and W_R (R-matrix multiplier).
FIS structure method	Subtractive clustering	Cluster radius 0.5; see Supplementary Note 2.
Number of fuzzy rules	9	Full rule base in Table 2 of main paper.
MFs per input	3	"Small", "Medium", "Large" for VE; "Negative", "Near zero", "Positive" for CVE.
MF type	Gaussian	Parameters $\{c_i, a_i\}$ and $\{d_j, b_j\}$; optimised by backprop.
Consequent type	Sugeno (1st order)	$f_{ij} = p_{ij}e + q_{ij}\Delta e + r_{ij}$; optimised by LSE.
Trainable parameters	78 total	12 premise + 2×27 consequent (one set per output).
Learning algorithm	Hybrid (LSE + backprop)	LSE for consequent; gradient-descent backprop for premise.

S3 1 Supplementary

Table S2: Power System Parameters

Supplementary Table S2. Power system component parameters for the Ethiopian 400 kV/230 kV Simulink model. Parameters derived from EEP technical specifications and IEC standard values for long HV lines. All per-unit quantities on component base unless stated otherwise.

Component / Parameter	Value	Unit	Notes
400 kV Transmission Lines (Pi Section Model)			
Resistance R	0.02	Ω/km	ACSR bundled conductor; IEC 60228 Class 2.
Inductance L	1.0	mH/km	Typical for 400 kV ACSR bundled line.
Capacitance C	11	nF/km	Shunt line capacitance.
Representative length	250	km	GERD–Addis Ababa corridor.
Rated voltage	400	kV (L-L, rms)	Nominal.
Thermal current limit	1 600	A	Per conductor.
230 kV Transmission Lines (Pi Section Model)			
Resistance R	0.04	Ω/km	Sub-transmission class.
Inductance L	1.2	mH/km	ACSR single conductor.
Capacitance C	9	nF/km	Shunt capacitance.
Representative length	120	km	Regional sub-transmission.
400 kV/230 kV Power Transformer			
Rated power	500	MVA	Three-phase bank.
Primary / Secondary voltage	400 / 230	kV	HV / MV windings.
Leakage reactance X_T	0.12	p.u.	On transformer MVA base.
Winding resistance	0.005	p.u.	On transformer base.
Tap range	±10	%	17 tap positions; step 1.25 %.
No-load losses	0.20	%	Of rated MVA.
Synchronous Generator (Hydropower Equivalent)			
Rated power	1 200	MVA	Aggregate equivalent: GERD+Gibe III.
Rated voltage	400	kV	
X_d (synchronous, d-axis)	1.10	p.u.	Round-rotor machine.
X_q (synchronous, q-axis)	1.05	p.u.	
X'_d (transient)	0.25	p.u.	
X''_d (sub-transient)	0.18	p.u.	

Continued...

Component / Parameter	Value	Unit	Notes
T'_{d0} (transient OC time const.)	7.5	s	
T''_{d0} (sub-transient OC)	0.05	s	
Inertia constant H	4.5	MWs/MVA	
Damping coefficient D	2.0	p.u.	
AVR type	IEEE Type AC1A	—	$K_A = 400$, $T_A = 0.02$ s.
PSS type	IEEE PSS1A	—	$K_w = 20$; speed input.
Composite Load (Addis Ababa Aggregate)			
Peak active demand	800	MW	
Peak reactive demand	400	MVAR	
Constant power (P) component	50	%	ZIP model.
Constant current (I) component	30	%	
Constant impedance (Z) component	20	%	
Nominal power factor	0.89	lagging	
Load increase rate (fault)	20	%/s	Applied from $t = 1$ s.
STATCOM			
Rated reactive power	±100	MVAR	Symmetric capability.
Connection voltage	230	kV	Load bus.
VSC response time constant	20	ms	Inner current control.
Coupling reactance	0.15	p.u.	On STATCOM base.
Rate limit	±20	MVAR/step	MPC hard constraint.
System Base Quantities			
System base MVA	1 000	MVA	
Base voltage HV	400	kV	
Base voltage MV	230	kV	
Simulation time step	50	μs	Variable-step `ode23t`.
MPC sampling period	100	ms	
Total simulation duration	6	s	

S4 1 Supplementary

Table S3: MPC and ANFIS Design Parameters

Supplementary Table S3. MPC and ANFIS design parameters with selection rationale. All MPC base parameters were selected by systematic iterative closed-loop simulation under nominal operating conditions (no disturbance) to yield stable voltage settling within 2 s with no overshoot. ANFIS parameters were determined by the subtractive clustering algorithm from training data.

Parameter	Value	Selection Rationale
MPC Parameters		
Prediction horizon N_p	10	Covers 1 s at $T_s = 100$ ms; captures dominant voltage time constants ($\sim$0.5 s) while keeping QP dimension tractable ($10n$ decision variables).
Control horizon N_u	3	Reduces QP degrees of freedom from $10m$ to $3m$ while retaining adequate control flexibility.
Sampling time T_s	100 ms	Satisfies Nyquist criterion for dominant dynamics; within typical SCADA communication cycle constraints.
$\mathbf{Q}_{\text{base}}$	$\text{diag}(10,\ldots)$	Smallest value yielding ≤ 2 s nominal settling; found by iterating $\mathbf{Q}_{\text{base}} = \text{diag}(q_0)$ with $q_0 \in \{1,2,5,10,20\}$.
$\mathbf{R}_{\text{base}}$	$\text{diag}(1)$	Moderate control-effort penalty; ANFIS multiplier W_R reduces this to 0.1 during fault onset.
Voltage bounds	[0.90, 1.10] p.u.	Emergency operating limits; enforced as hard QP inequality constraints at all prediction steps.
STATCOM Q bounds	$[-100, +100]$ MVAR	Physical device limits; box constraints on control input.
ΔQ rate limit	± 20 MVAR/step	Prevents STATCOM mechanical stress; control increment constraint.
QP solver	`quadprog`	MATLAB MPC Toolbox, active-set method.
Mean QP solve time	8.3 ms	Intel Core i7-12700, 32 GB RAM, MATLAB R2023b.
ANFIS Parameters		
Input 1: VE range	[0, 1]	Normalised voltage error $V_{\text{ref}} - V_{\text{actual}}$.
Input 2: CVE range	[0, 1]	Normalised $d(\text{VE})/dt$.
Clustering method	Subtractive	Cluster radius 0.5; see Note 2.
Number of rules	9	From 3×3 partitioning of input space.
W_Q output range	[0.5, 8.0]	Min: nominal weight ($k = 1$); max: $16\times$ nominal.
W_R output range	[0.1, 2.0]	Min: $0.05\times$ nominal; max: $2\times$ nominal.
ANFIS inference time	0.4 ms	Per control step on same hardware as QP.
Total control cycle	8.7 ms	Well within 100 ms sampling period.

S5 1 Supplementary

Note 1: ANFIS Layer Mathematics

The ANFIS employed in this work is a five-layer adaptive network implementing a Sugeno-type fuzzy inference system. This note provides the complete mathematical specification of each layer, complementing the summary in the Methods section of the main paper.

S5.1 Layer 1: Fuzzification

Layer 1 computes the membership grade of each input to each linguistic term. For the two inputs e (voltage error, VE) and Δe (change in voltage error, CVE), Gaussian membership functions are used:

$$O_i^1(e) = \mu_{A_i}(e) = \exp\left[-\frac{1}{2}\left(\frac{e-c_i}{a_i}\right)^2\right], \quad i = 1,2,3 \tag{S1}$$

$$O_j^1(\Delta e) = \mu_{B_j}(\Delta e) = \exp\left[-\frac{1}{2}\left(\frac{\Delta e-d_j}{b_j}\right)^2\right], \quad j = 1,2,3 \tag{S2}$$

where c_i and a_i are the centre and width of the i-th Gaussian for input e, and d_j and b_j are the corresponding parameters for Δe. All four sets of parameters $\{c_i, a_i, d_j, b_j\}$ are optimised during training by the gradient-descent backpropagation component of the hybrid learning algorithm.

S5.2 Layers 2–3: Rule Firing and Normalisation

Layer 2 computes the firing strength w_{ij} of each of the 9 rules using the product (fuzzy AND) operator:

$$O_{ij}^2 = w_{ij} = \mu_{A_i}(e) \times \mu_{B_j}(\Delta e), \quad i, j \in \{1,2,3\} \tag{S3}$$

Layer 3 normalises the firing strengths across the full rule base:

$$O_{ij}^3 = \bar{w}_{ij} = \frac{w_{ij}}{\sum_{k=1}^{3}\sum_{l=1}^{3} w_{kl}} \tag{S4}$$

S5.3 Layer 4: Consequent Layer

Layer 4 applies first-order Sugeno linear consequent parameters $\{p_{ij}, q_{ij}, r_{ij}\}$ to compute each rule's weighted output:

$$O_{ij}^4 = \bar{w}_{ij} f_{ij} = \bar{w}_{ij}(p_{ij} e + q_{ij} \Delta e + r_{ij}) \tag{S5}$$

The consequent parameters $\{p_{ij}, q_{ij}, r_{ij}\}$ are optimised by the least-squares estimation (LSE) component of the hybrid learning algorithm.

S5.4 Layer 5: Output Summation

Layer 5 computes the final crisp output (W_Q or W_R) as the weighted average:

$$\text{Output} = \frac{\sum_{i=1}^{3}\sum_{j=1}^{3} w_{ij} f_{ij}}{\sum_{i=1}^{3}\sum_{j=1}^{3} w_{ij}} \tag{S6}$$

The two outputs W_Q and W_R are computed by separate sets of consequent parameters $\{p_{ij}^Q, q_{ij}^Q, r_{ij}^Q\}$ and $\{p_{ij}^R, q_{ij}^R, r_{ij}^R\}$ respectively, sharing the same premise parameters $\{c_i, a_i, d_j, b_j\}$.

S6 1 Supplementary Note 2: Subtractive Clustering

Subtractive clustering[1] was used to generate the initial FIS structure from the training data. The algorithm treats each data point as a potential cluster centre and estimates the likelihood of each point being a cluster centre based on the density of surrounding data points. Given normalised input data $\mathbf{x}_k \in [0,1]^2$, the density measure for point i is:

$$D_i = \sum_k \exp\left(-\frac{\|\mathbf{x}_i - \mathbf{x}_k\|^2}{(r_a/2)^2}\right) \tag{S7}$$

where $r_a = 0.5$ is the cluster radius (selected to balance rule parsimony against coverage). The point with the highest density D_i^* is selected as the first cluster centre. Data points within radius $r_b = 1.5 r_a$ of this centre are suppressed. The process repeats until the ratio of the next candidate's density to the first cluster's density falls below a threshold ($\varepsilon_l = 0.15$). This procedure identified 9 cluster centres in the normalised input space, each corresponding to one fuzzy rule, and determined the initial Gaussian membership function parameters $\{c_i, a_i, d_j, b_j\}$ from the cluster positions and radii.

S7 1 Supplementary Note 3: Simulation-to-Implementation

While the simulation results demonstrate compelling performance, several practical factors must be addressed before field deployment.

Communication latency. SCADA communication cycles in Ethiopian EEP substations range from approximately 100–500 ms. Measurement latency of this magnitude introduces a delay in the CVE (rate-of-change) estimate, which is computed from consecutive VE samples. At the MPC sampling period of $T_s = 100$ ms, a 100 ms latency degrades the CVE estimate by introducing a one-step lag; a 300 ms latency would reduce the effective CVE bandwidth by 67 %. Mitigation strategies include predictive filtering of VE (e.g., Kalman-based state estimation incorporating network dynamics) and adaptive sampling-period adjustment based on measured latency.

Hardware-in-the-loop validation. Before field deployment, the ANFIS-MPC should be validated on a real-time HIL platform (e.g., OPAL-RT OP5700 or Typhoon HIL 604) interfaced with the MATLAB/Simulink model. The 8.7 ms mean control cycle comfortably fits within the 100 ms period on a dedicated industrial control processor (e.g., Bachmann MPC240).

Linearised model accuracy. The MPC's internal linearised state-space model degrades in accuracy as the system deviates from the nominal operating point during severe voltage collapse. The ANFIS adaptive weighting provides partial implicit compensation; however, for improved accuracy, future implementations should consider: (i) adaptive re-linearisation triggered when voltage deviation exceeds a threshold (e.g., $|\mathrm{VE}| > 0.1$ p.u.); (ii) Koopman operator-based predictors that capture global nonlinear dynamics in a linear framework; or (iii) ANFIS as the MPC's internal prediction model.

S8 1 Supplementary References

S8 1 References

[1] Chiu, S. L. Fuzzy model identification based on cluster estimation. *J. Intell. Fuzzy Syst.* **2**, 267–278 (1994).

[2] Kundur, P. *Power System Stability and Control* (McGraw-Hill, New York, 1994).